

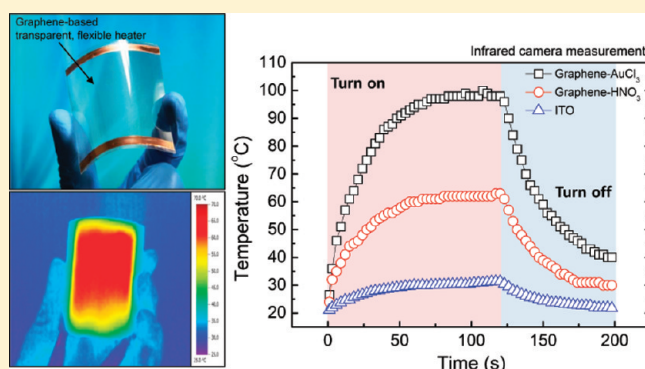
## High-Performance Graphene-Based Transparent Flexible Heaters

Junmo Kang,<sup>†</sup> Hyeongkeun Kim,<sup>||</sup> Keun Soo Kim,<sup>‡</sup> Seoung-Ki Lee,<sup>‡</sup> Sukang Bae,<sup>†</sup> Jong-Hyun Ahn,<sup>†,‡</sup> Young-Jin Kim,<sup>†,§</sup> Jae-Boong Choi,<sup>\*,†,§</sup> and Byung Hee Hong<sup>\*,†,#</sup><sup>†</sup>SKKU Advanced Institute of Nanotechnology (SAINT) and Center for Human Interface Nano Technology (HINT), <sup>‡</sup>School of Advanced Materials Science and Engineering, <sup>§</sup>School of Mechanical Engineering, Sungkyunkwan University, Suwon, 440-746, Korea<sup>||</sup>Electronic Materials and Device Research Center, Korea Electronics Technology Institute (KETI), Seongnam, 432-816, Korea<sup>‡</sup>Department of Physics and Graphene Research Institute, Sejong University, Seoul, 143-747, Korea<sup>#</sup>Department of Chemistry, Seoul National University, Seoul, 151-742, Korea

## Supporting Information

**ABSTRACT:** We demonstrate high-performance, flexible, transparent heaters based on large-scale graphene films synthesized by chemical vapor deposition on Cu foils. After multiple transfers and chemical doping processes, the graphene films show sheet resistance as low as  $\sim 43$  Ohm/sq with  $\sim 89\%$  optical transmittance, which are ideal as low-voltage transparent heaters. Time-dependent temperature profiles and heat distribution analyses show that the performance of graphene-based heaters is superior to that of conventional transparent heaters based on indium tin oxide. In addition, we confirmed that mechanical strain as high as  $\sim 4\%$  did not substantially affect heater performance. Therefore, graphene-based, flexible, transparent heaters are expected to find uses in a broad range of applications, including automobile defogging/deicing systems and heatable smart windows.

**KEYWORDS:** Graphene, transparent, flexible, heater, chemical vapor deposition, layer-by-layer doping



Graphene has attracted a tremendous amount of attention over the past few years because of its outstanding electrical,<sup>1,2</sup> mechanical,<sup>3,4</sup> and chemical<sup>5,6</sup> properties. Various efforts have been made to use these fascinating properties for macroscopic applications, such as transparent conducting films that can replace indium tin oxide (ITO).<sup>7–10</sup> Recent advances in graphene growth techniques have enabled the roll-to-roll synthesis of high-quality graphene films as large as 30 in. in diagonal,<sup>11</sup> and the field expects to soon realize the industrial production of graphene conducting films for macroscopic applications, including displays, solar cells, and transparent heaters.

A transparent heater is very useful for clearing automobile windows, mirrors, and displays, as well as ensuring the fast response of electronic devices under extreme environmental conditions. ITO film has been widely used as a transparent heater, but it not only exhibits a slow thermal response but also requires complicated fabrication processes that rely on rare indium sources, resulting in higher production costs.<sup>12,13</sup> For this reason, there have been many efforts to replace ITO films with a new type of transparent conducting film, such as single-walled carbon nanotube (SWNT) sheets, as demonstrated by Yoon et al.<sup>14</sup> While transparent SWNT films show a rapid thermal response and have a better heating performance than ITO films, their dispersion process requires strong acid treatments and surfactants, which limit the conductivity of SWNT-based

conducting films. In addition, the difficulty in removing semi-conducting SWNTs hinders the enhancement of their optical transmittance ( $T_r$ ) at a given sheet resistance ( $R_s = \sim 180$  Ohm/sq at  $T_r = 90\%$ ).<sup>15</sup> Thus, we suggest the use of large-scale graphene films synthesized by chemical vapor deposition (CVD) methods for transparent heaters. Graphene demonstrates exceptional optoelectronic properties that are superior to those of previously used transparent conducting materials ( $R_s = \sim 43$  Ohm/sq at  $T_r = 89\%$ ).<sup>16</sup> The outstanding thermal conductivity of graphene films<sup>17–20</sup> provides another advantage for using graphene in transparent heaters; it quickly delivers heat to the environment. This results in a faster heating rate and a more homogeneous temperature distribution. In addition, the flexibility of graphene further allows its facile application to a curved window surface or as a rollable screen because it can be prepared as an attachable film structure combined with polymer substrates.

For the large-scale production of high-quality graphene films for heater applications, the CVD system is used, allowing the synthesis of a monolayer graphene film on a roll of Cu foil. Figure 1 shows a schematic of the fabrication procedure for transparent flexible graphene films with layer-by-layer doping

Received: July 7, 2011

Revised: November 8, 2011

Published: November 14, 2011

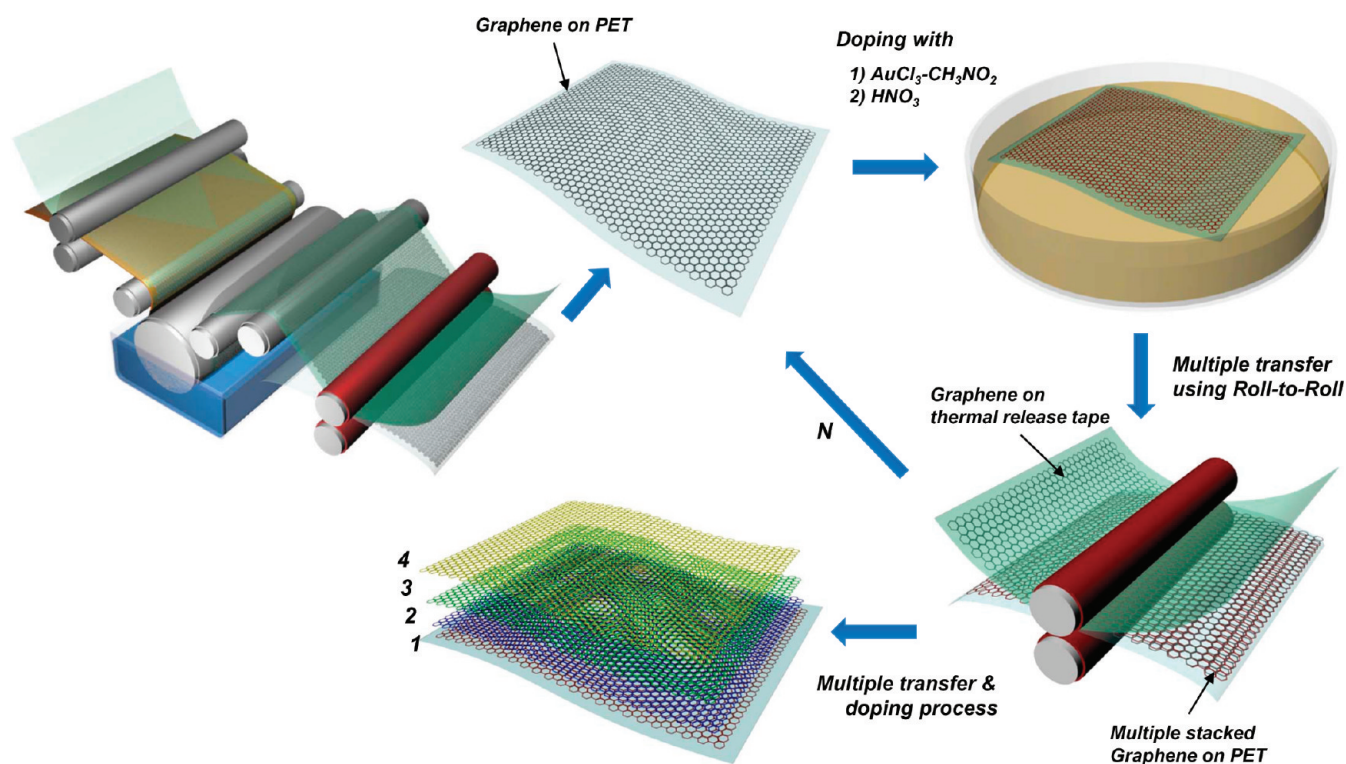


**Figure 1.** A schematic of the fabrication procedures for preparing transparent flexible graphene films with layer-by-layer doping methods. The interlayer-doped graphene films are exposed to two wet chemical p-dopants, such as  $\text{AuCl}_3\text{-CH}_3\text{NO}_2$  and  $\text{HNO}_3$ , after each layer is transferred, leading to the low sheet resistance as low as  $\sim 43 \text{ Ohm/sq}$  with  $\sim 89\%$  optical transmittance.

methods. A roll of Cu foil is inserted into a quartz tube and heated to  $1000 \text{ }^\circ\text{C}$  with  $\text{H}_2$  flowing at 2 sccm at 20 mTorr. After annealing for 30 min without changing the flow rate or pressure, a gas mixture of  $\text{CH}_4$  and  $\text{H}_2$  is flowed at 400 mTorr with rates of 28 and 2 sccm for 30 min, respectively. Finally, the sample is rapidly cooled to room temperature with a mixed flow of  $\text{H}_2$  and He under a pressure of 400 mTorr. After growth, the graphene film grown on the Cu foil is transferred to the target substrate by using a roll-to-roll process, as suggested by a previous paper.<sup>11</sup> There are three steps in the roll-to-roll transfer as illustrated in Figure 1. First, the thermal release tape (Nitto Denko Co.) is attached to the graphene film on the Cu foil. After etching the Cu foil in a bath filled with Cu etchant, the graphene film is then rinsed with deionized water to remove residual etchant. The graphene film on the polymer support is inserted between the rollers, together with a target substrate, and exposed to mild heat ( $140 \text{ }^\circ\text{C}$ ), resulting in the transfer of the graphene film from the polymer support to the target substrate. In order to improve the electrical quality of graphene films with high optical transmittance, we carried out multiple stacking processes and a wet-chemical doping process. We used gold(III) chloride-nitromethane ( $\text{AuCl}_3\text{-CH}_3\text{NO}_2$ , 0.025 M) and nitric acid ( $\text{HNO}_3$ , 16 M) on graphene films to compare the difference in their heating performance after treatment. First, graphene film on a polyethylene-terephthalate (PET) substrate was immersed in the dopant solution for 5 min. After the doping process, the graphene film was placed with another graphene film on thermal release tape and exposed to heat, fabricating multiple stacked graphene films. By repeating these steps on the same substrate, interlayer-doped graphene films can be prepared by a roll-to-roll process, as demonstrated by Bae and colleagues.<sup>11</sup> Supplementary Figure S1

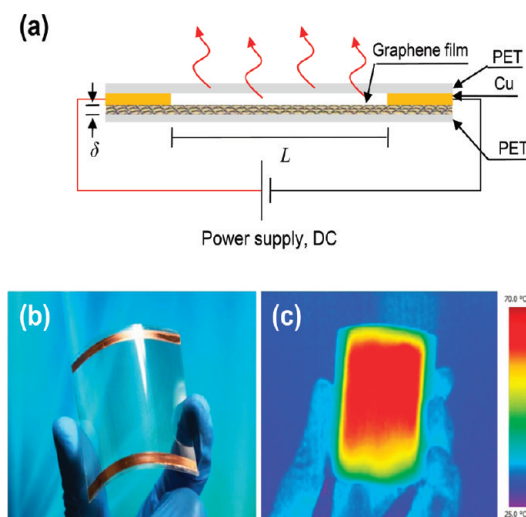


**Figure 2.** (a) A schematic structure of a transparent, flexible graphene heater combined with a plastic substrate and Cu electrodes. (b) An optical image of the assembled graphene-based heater showing its outstanding flexibility. (c) An infrared picture of the assembled graphene-based heater while applying an input voltage under bending conditions.

(Supporting Information) shows the electrical and optical characterizations of graphene films as a function of layer-by-layer doping with (a)  $\text{AuCl}_3\text{-CH}_3\text{NO}_2$  and (b)  $\text{HNO}_3$ . The optical transmittance at  $\lambda = 550 \text{ nm}$  is usually decreased by 2.3%<sup>21</sup> for each additional transfer. Finally, we fabricated a sheet with a resistance as low as  $\sim 43 \text{ Ohm/sq}$  and a transmittance of  $\sim 89\%$

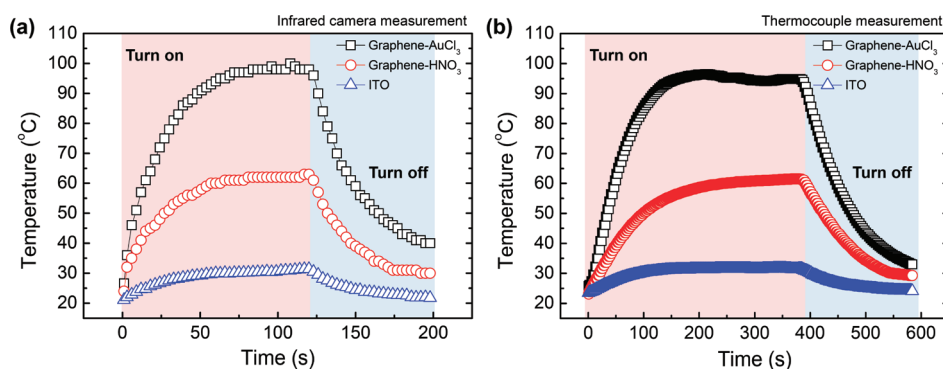


**Figure 3.** The temperature profiles of graphene-based heaters with two different doping agents and an ITO-based heater, measured by (a) an infrared scanner (Testo 881) and (b) a thermocouple (K-type).

with four layers of graphene film and  $\text{AuCl}_3\text{-CH}_3\text{NO}_2$  doping (see supplementary Figure S1a in Supporting Information).

Figure 2a illustrates the schematic structure of a graphene-based heater. The graphene films were located within PET substrates. The “closed” configuration reduced heat loss because the top PET was described as a thermal barrier containing the heat generated from the graphene films.<sup>14</sup> The copper layer is used to enhance the contact with graphene at the edge. The input voltage is supplied to the graphene-based heater between Cu electrodes separated by a distance  $L$ . The power consumption of a graphene film heater can be calculated by basic electrical formulas. The equations governing the total power consumption  $P$  and resistance  $R$  of operating a graphene heater can be written as

$$P = I^2R \quad (1)$$

$$R = \rho \left( \frac{L}{A} \right) = \rho \left( \frac{L}{\delta W} \right) \quad (2)$$

where  $I$  is the current passing through the graphene heater,  $\rho$  is the resistivity, and  $A$  is the area of the graphene heater, consisting of thickness  $\delta$  and width  $W$ . We assumed that the thickness of a single layer was 0.334 nm, the same as the interlayer spacing in graphite.<sup>7,11</sup> The resistivity of graphene film is given by  $\rho = G(V/I)$ , where  $V$  is the voltage and a geometric factor  $G$  is obtained as  $G = 4.5324\delta$ .<sup>22</sup> By a four-point probe method, we measured the resistance  $R$ , which is shown in Supporting Information Figure S1a,b. The input voltage was supplied up to 12 V. We calculated the power consumption values based on the theoretical and experimental data for graphene doped with  $\text{AuCl}_3\text{-CH}_3\text{NO}_2$  (3.24 W) or  $\text{HNO}_3$  (1.42 W) with and ITO film (0.58 W) (Supplementary Table 1 in Supporting Information). Figure 2b shows a photograph of the fabricated graphene-based heater, which shows outstanding flexibility. Figure 2c is an image of the graphene heater taken by an infrared camera while the graphene was undergoing bending deformation. This graphene-based heater showed uniform heat performance under bending conditions, as we will discuss later.

Figure 3a,b depicts the time-dependent temperature of the two types of graphene-based heaters treated with different dopants and an ITO-based heater. The size of the heaters was  $4 \times 4 \text{ cm}^2$ . The temperature responses of the heaters were measured by an infrared camera (Figure 3a). We applied 12 V to both the graphene heater and the ITO heater using a DC power supply (Agilent, 33250A), which can monitor the electrical current flowing through the heaters. We collected the

temperature responses of the heaters every three seconds. The response time, which is the time it takes for the heater to reach a steady-state temperature from room temperature, did not depend on the type of heater. The response time can be attributed to the additional thermal mass,<sup>14</sup> which in this case is a PET layer covering the film heater. PET layer covers both the graphene-based and ITO-based heaters, acting as a thermal barrier against atmospheric environments. In these experimental results, graphene heaters doped with  $\text{AuCl}_3\text{-CH}_3\text{NO}_2$  exhibited the better performance with higher steady state temperature up to 100 °C at 12 V, compared to 65 °C for  $\text{HNO}_3$ -doped graphene heaters. This comparison reveals that the electrical conductivity of graphene films is important to achieve the better performances of graphene heaters. In order to compare the heat performance and the distribution of graphene heaters, we fabricated an ITO heater with a sheet resistance of  $\sim 392 \text{ Ohm/sq}$  and an optical transmittance of 95.6%. The maximum temperature of the ITO heater was 31.4 °C at steady state and 12 V. We also performed statistical analysis of temperature distribution on graphene-based and ITO-based heaters as seen in Supporting Information Figure S2. The temperature distribution of the graphene heaters was more uniform than that of the ITO heaters. In addition, we measured the power consumptions of the  $\text{HNO}_3$ -doped graphene heater working at 12 V and the ITO-based heater at 20 V, which are 1.42 and 1.56 W, respectively. Although the power consumptions of two different heaters are similar, the graphene-based heater shows the higher steady-state temperature with better heating performance. Figure 3b shows the temperature response measured with a thermocouple. Although the thermocouple-based measurement shows a slow response because of the slow heat propagation, there was little difference between the thermocouple measurement and the infrared-based measurement, which validates the data obtained from the infrared measurement. The time-dependent temperature profiles and heat distribution analyses show that the performance of graphene-based heaters is superior to that of conventional transparent ITO heaters. We made another larger device to demonstrate the temperature distribution over a larger area (Supporting Information Figure S4). The size of the large-scale graphene heater was  $9 \times 9 \text{ cm}^2$ . The overall temperature response was lower than for the smaller device because of both the higher sheet resistance than doped graphene heaters and the increase in the heating area; the device reached 55 °C for 30 V. However, most area over graphene in large-scale heater exhibit very uniform color distribution, indicating the uniform temperature distribution over the graphene film. The surface temperature could

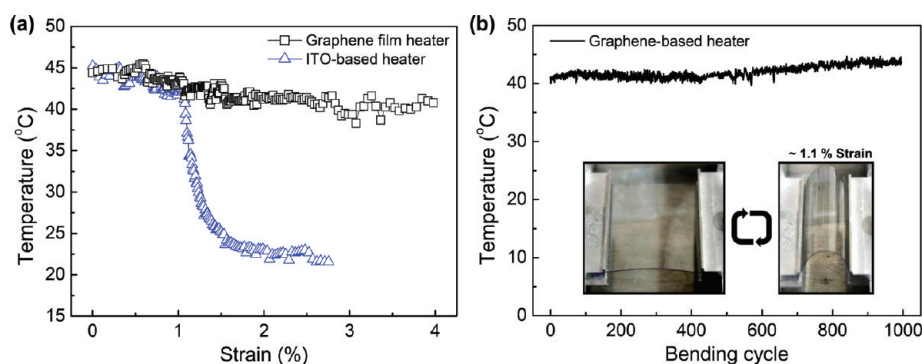


**Figure 4.** Mechanical characterizations of the graphene-based heater, including (a) variations in the temperature of a graphene-based heater compared with an ITO-based heater as a function of bending strain and (b) mechanical stability test results of the graphene-based heater. The four-layer graphene film on a 188  $\mu\text{m}$  thick PET substrate was bent 1000 times with 1.1% strain.

decrease as the heating area increases. Nevertheless, when desired temperature can be set by modifying the sheet resistance using chemical doping and multiple transfer process, the graphene could be produced into large-scale heater. These results demonstrate that graphene-based heaters could be applied as transparent heaters for a vehicle or a smart window system.

To understand the heat performance of graphene film heaters under bending conditions, we describe experimental results obtained from changing the temperature of the graphene-based heaters and the ITO-based heater under mechanical strain and bending cycles. Figure 4a demonstrates the electromechanical properties of graphene-based heaters and ITO-based heater. Bending strain was applied to four-layer graphene films transferred to a PET (188  $\mu\text{m}$ ) and ITO coated on a PET (130  $\mu\text{m}$ ). The strain can be calculated from the following equation<sup>23</sup>

$$\varepsilon = \left( \frac{\delta_s + \delta_f}{2R_C} \right) \frac{(1 + 2\eta + \chi\eta^2)}{(1 + \eta + \chi\eta + \chi\eta^2)} \quad (3)$$

where  $\eta = \delta_f/\delta_s$ ,  $\chi = Y_f/Y_s$ , and  $R_C$  is the bending radius.  $Y$  is Young's modulus. The subscripts  $s$  and  $f$  indicate the substrate (PET) and film (graphene). Typically, approximately 1.2% strain for an ITO-coated PET sample with a thickness of 130  $\mu\text{m}$  is regarded as a failure strain.<sup>24</sup> Unlike an ITO-based heater, which easily breaks at an approximate strain of 1.1%, in our experiments, the graphene-based heater resisted a strain of up to 4%.<sup>7</sup> The temperature of the graphene-based heater changed by 9%, which was observed for a range of strains up to  $\sim 4\%$  (corresponding to a bending radius of 2.36 mm). In addition to the experiments in the mechanical stability of graphene-based heater we have performed bending stability test (Figure 4b). The bending test was repeated 1000 times during application of the input voltage. The bending rate was one cycle per 20 s (0.05 Hz). The lower inset in Figure 4b shows optical images of the bent device under  $\sim 1.1\%$  strain, which was the threshold strain for ITO-coated PET. Only small changes in temperature deviation of approximately 1.02  $^\circ\text{C}$  were detected over the complete mechanical stability experiment. Therefore, the excellent mechanical properties of graphene films can be applied to produce transparent, flexible heaters.

In summary, we have developed a flexible and transparent heater composed of graphene films. We fabricated multiple stacked graphene films using a roll-to-roll method and prepared interlayer doped graphene films using two wet chemical dopants,  $\text{AuCl}_3\text{-CH}_3\text{NO}_2$  and  $\text{HNO}_3$ , resulting in a low sheet resistance

ideal for low-voltage heaters. The temperature response and heat distribution results show that the performance of graphene-based heaters is superior to that of conventional ITO-based transparent heaters. In particular, the graphene-based heaters are mechanically stable against large bending deformations, which is suitable for automobile defogging/deicing systems and heatable smart windows.

## ■ ASSOCIATED CONTENT

**S Supporting Information.** Additional information and figures. This material is available free of charge via the Internet at <http://pubs.acs.org>.

## ■ AUTHOR INFORMATION

### Corresponding Author

\*E-mail: (B.H.H.) [bunghee@snu.ac.kr](mailto:bunghee@snu.ac.kr); (J.-B.C.) [boong33@skku.edu](mailto:boong33@skku.edu).

## ■ ACKNOWLEDGMENT

This research was supported by Basic Science Research Program (2011K000615, 2011-0017587, 2011-0006270, 2010-0028037, 2011-0006268), Global Research Lab. (GRL) Program (2011-0017587), Priority Research Centers Program (2011-0018395) through the National Research Foundation of Korea (NRF) funded by the Ministry of Education, Science, and Technology. This work (000-437-010-110) was supported by Business for Cooperative R&D between Industry, Academy, and Research Institute funded Korea Small and Medium Business Administration in 2010.

## ■ REFERENCES

- (1) Geim, A. K.; Novoselov, K. S. *Nat. Mater.* **2007**, *6*, 183–191.
- (2) Novoselov, K. S.; Geim, A. K.; Morozov, S. V.; Jiang, D.; Zhang, Y.; Dubonos, S. V.; Grigorieva, I. V.; Firsov, A. *Science* **2004**, *306*, 666–669.
- (3) Lee, C.; Wei, X.; Kysar, J. W.; Hone, J. *Science* **2008**, *321*, 385–388.
- (4) Ruiz-Vargas, C. S.; Zhuang, H. L.; Huang, P. Y.; van der Zande, A. M.; Garg, S.; McEuen, P. L.; Muller, D. A.; Hennig, R. G.; Park, J. *Nano Lett.* **2011**, *11*, 2259–2263.
- (5) Elias, D. C.; Nair, R. R.; Mohiuddin, T. M.; Morozov, S. V.; Blake, P.; Halsall, M. P.; Ferrari, A. C.; Boukhalov, D. W.; Katsnelson, M. I.; Geim, A. K.; Novoselov, K. S. *Science* **2009**, *323*, 610–613.

- (6) Wang, X.; Li, X.; Zhang, L.; Yoon, Y.; Weber, P. K.; Wang, H.; Guo, J.; Dai, H. *Science* **2009**, *324*, 768–771.
- (7) Kim, K. S.; Zhao, Y.; Jang, H.; Lee, S. Y.; Kim, J. M.; Kim, K. S.; Ahn, J. H.; Kim, P.; Choi, J. Y.; Hong, B. H. *Nature* **2009**, *457*, 706–710.
- (8) Li, X. S.; Cai, W. W.; An, J. H.; Kim, S.; Nah, J.; Yang, D. X.; Piner, R. D.; Velamakanni, A.; Jung, I.; Tutuc, E.; Banerjee, S. K.; Colombo, L.; Ruoff, R. S. *Science* **2009**, *324*, 1312–1314.
- (9) Reina, A.; Jia, X.; Ho, J.; Nezich, D.; Son, H.; Bulovic, V.; Dresselhaus, M. S.; Kong, J. *Nano Lett.* **2009**, *9*, 30–35.
- (10) Lee, Y.; Bae, S.; Jang, H.; Jang, S.; Zhu, S.; Sim, S.; Song, Y. I.; Hong, B. H.; Ahn, J. H. *Nano Lett.* **2010**, *10*, 490–493.
- (11) Bae, S.; Kim, H.; Lee, Y.; Xu, X.; Park, J.; Zheng, Y.; Balakrishnan, J.; Lei, T.; Ri Kim, H.; Song, Y. I.; Kim, Y.; Kim, K. S.; Ozyilmaz, B.; Ahn, J. H.; Hong, B. H.; Iijima, S. *Nat. Nanotechnol.* **2010**, *5*, 574–578.
- (12) Belton C. G.; Garreau, L. European Patent, 1,612,5252006.
- (13) Alder, R. F. U.S. Patent 6,358,138, 2002.
- (14) Yoon, Y. H.; Song, J. W.; Kim, D.; Kim, J.; Park, J.; Oh, S.; Han, C. S. *Adv. Mater.* **2007**, *19*, 4284–4287.
- (15) Geng, H.-Z.; Kim, K. K.; So, K. P.; Lee, Y. S.; Chang, Y. K.; Lee, Y. H. *J. Am. Chem. Soc.* **2007**, *129*, 7758–7759.
- (16) Bonaccorso, F.; Sun, Z.; Hasan, T.; Ferrari, A. C. *Nat. Photonics* **2010**, *4*, 611–622.
- (17) Seol, J. H.; Jo, I.; Moore, A. L.; Lindsay, L.; Aitken, Z. H.; Pettes, M. T.; Li, X. S.; Yao, Z.; Huang, R.; Broido, D.; Mingo, N.; Ruoff, R. S.; Shi, L. *Science* **2010**, *328*, 213–216.
- (18) Balandin, A. A.; Ghosh, S.; Bao, W.; Calizo, I.; Teweldebrhan, D.; Miao, F.; Lau, C. N. *Nano Lett.* **2008**, *8*, 902–907.
- (19) Balandin, A. A. *Nat. Mater.* **2011**, *10*, 569–581.
- (20) Cai, W.; Moore, A. L.; Zhu, Y.; Li, X.; Chen, S.; Shi, L.; Ruoff, R. S. *Nano Lett.* **2010**, *10*, 1645–1651.
- (21) Nair, R. R.; Blake, P.; Grigorenko, A. N.; Novoselov, K. S.; Booth, T. J.; Stauber, T.; Peres, N. M. R.; Geim, A. K. *Science* **2008**, *320*, 1308.
- (22) Smits, F. M. *Bell Syst. Tech. J.* **1958**, *37*, 711–718.
- (23) Suo, Z.; Ma, E. Y.; Gleskova, H.; Wagner, S. *App. Phys. Lett.* **1999**, *74*, 1177–1179.
- (24) Bouten, P. C. P. Failure test for brittle conductive layers on flexible display substrates, Eurodisplay 2002. *J. Soc. Inf. Disp.* **2002**, 313–316.